THE ASTROPHYSICAL JOURNAL, 416:251–255, 1993 October 10

THE CRAB NEBULA'S COSMIC-RAY ACCELERATION ZONE REVEALED

P. P. KRONBERG,[1] H. LESCH,[1,2] P. F. ORTIZ,[1] AND M. F. BIETENHOLZ[1]

Received 1993 January 22; accepted 1993 April 2

ABSTRACT

We analyze and discuss the geometrical and physical properties of the geometrically coherent, and the time-variable radio spectral index perturbations near the center of the Crab Nebula recently discovered by Bietenholz & Kronberg.

Although the detailed explanation of the three-dimensional geometry of the α perturbations is not yet clear, we propose that they are the sites of electron acceleration by MHD waves. The MHD waves are also the cause of the isotropization of the plasma flow outside the inner "emission hole" at the Crab's center, and we show how the MHD turbulence *near* the shock produces the observed spectral index, $\alpha \sim 0$ in the α-ridges, and a somewhat steeper spectrum further out in the supernova remnant, as is also observed.

We also suggest a physical explanation for the "persistent" magnetic field cell structure, and the typical 10″ cell size as determined from the projected magnetic field maps of Bietenholz & Kronberg.

Subject headings: acceleration of particles — cosmic rays — ISM: individual (Crab Nebula) — MHD

1. INTRODUCTION

A remarkable image which reveals for the first time the three-dimensional geometry of the Crab Nebula's particle acceleration zone has recently been published and discussed by Bietenholz & Kronberg (1992). It is one of a series of papers analyzing a new generation of multifrequency, precision radio images of the Crab Nebula (SN 1054) at arcsecond resolution (Bietenholz & Kronberg 1990, 1991; Bietenholz et al. 1991). These were taken with all configurations of the NRAO Very Large Array (VLA)[3] between 1987 July and 1988 March.

The new VLA images reveal organized, arcsecond-scale radio "wisps" within the inner supernova remnant (Fig. 1 [Pl. 3]). The radio "wisps" constitute a series of arclike features of the radio continuum emission which are most clearly visible as perturbations of the radio spectral index α, in that they have a significantly *flatter* α than the body of the nebula. These features have a thickness ≤ 0.01 pc (3×10^{16} cm), and are continuous over ~ 0.6 pc (Fig. 1 and Bietenholz & Kronberg 1992). Their flatter spectral index indicates that they are sites of freshly accelerated cosmic ray electrons. Their (projected) geometrical form indicates that, in three-dimensional space, they are not sheets, but rather *tubes*, or *filaments*, which fill a relatively small fraction of the inner nebula's volume. Bietenholz & Kronberg (1992) estimated that their *volume* emissivity at 1.5 GHz is enhanced by a factor of between 5 and 80 relative to the local ambient radio continuum emission.

The radio wisps occur in a zone close to the optical wisps originally discovered by Scargle (1968, 1969). However, contrary to the optical wisp variability on time scales of months, the radio wisps change their structure more slowly, over times ≥ 1 yr (Bietenholz & Kronberg 1992). They appear to be portions of *ordered, circularly symmetric* features which we are seeing tilted to our line of sight. They provide us with the first opportunity to examine the three-dimensional structure of the Crab's inner particle acceleration zone. The next section describes this analysis, and in the following section we briefly discuss implications of these new results for models of relativistic particle acceleration and energy transport from the pulsar into the observed Nebula.

3. THE THREE-DIMENSIONAL MORPHOLOGY OF THE RADIO WISPS

We have devised image analysis techniques to explore the three-dimensional geometry of the *spectral index* (α) perturbation zones. The purpose is an attempt to "discover," with minimum a priori bias, the true shape of the particle acceleration zones which conform with the data. The computer search consisted in first finding the local maxima in the spectral index map. The maxima were searched in two sets of orthogonal directions: one set oriented north-south and east-west and the other rotated 45° from the first one. The standard deviation of the data points along each search line was used as a measure of the noise, which in turn was used to choose a threshold in the selection of the local maxima. Once the local maxima were found, an algorithm was applied to search for contiguous "ridge lines" among the maxima.

These procedures confirm the following: (1) several spatially contiguous "enhanced α-zones" exist within the inner 0.6 pc of the supernova remnant, and (2) that they appear to be projections of a simple three-dimensional geometry. The search was performed with various trial levels of statistical significance to gain confidence in its ability to reliably identify real features. It was combined with a second technique, which is to transform the α-ridge image into an (r, θ) plot, where r is the radial distance from the pulsar position, and θ is the position angle (measured eastward from north). This is shown in Figure 2, which clearly indicates that there are distinct, contiguous features in (r, θ) space. A circle in the plane of the sky, and centered on the pulsar transforms into a straight line of zero slope in (r, θ) space, and a face-on spiral would appear as a line of constant slope. Offset (from the pulsar position) circular fea-

[1] Department of Astronomy, University of Toronto, 60 St. George Street, Toronto, Canada M5S 1A7.

[2] Also Canadian Institute of Theoretical Astrophysics. Postal address: Max-Planck-Institut für Radioastronomie, Auf dem Hügel 69, D-5300 Bonn 1, Germany.

[3] The National Radio Astronomy Observatory is operated by Associated Universities, Inc., under Cooperative Agreement with the National Science Foundation.

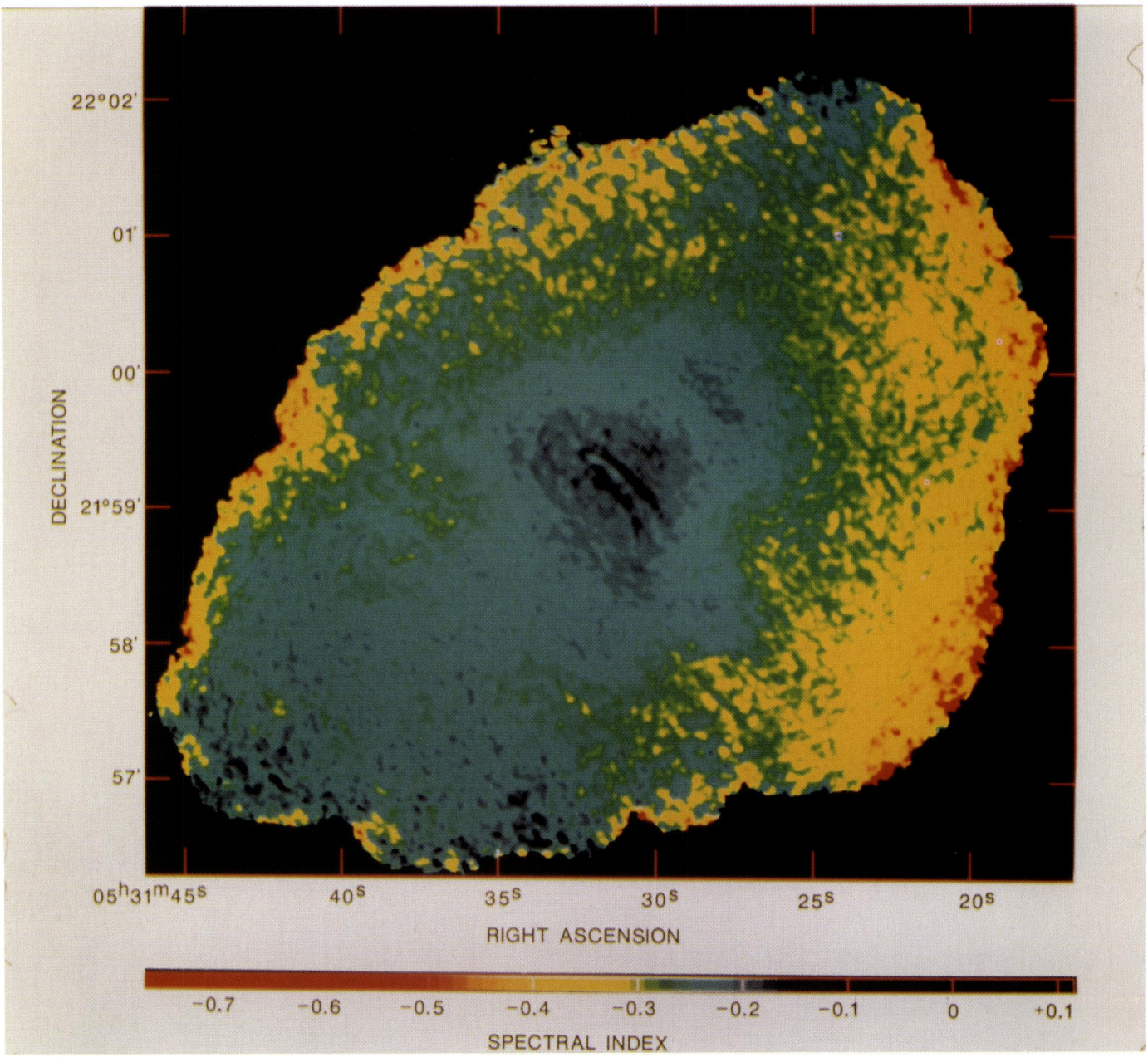

FIG. 1.—Image of the radio spectral index distributing between 1.4 and 4.89 GHz over the Crab Nebula, as measured by Bietenholz & Kronberg. Regular arclike features can be seen near the center of the Crab Nebula at the resolution of 1".8. Darker blue indicates increasingly flat/inverse spectral index. The large-scale steepening of spectral index toward the edge could be an artifact caused by missing short interferometer spacings.

KRONBERG et al. (see 416, 251)

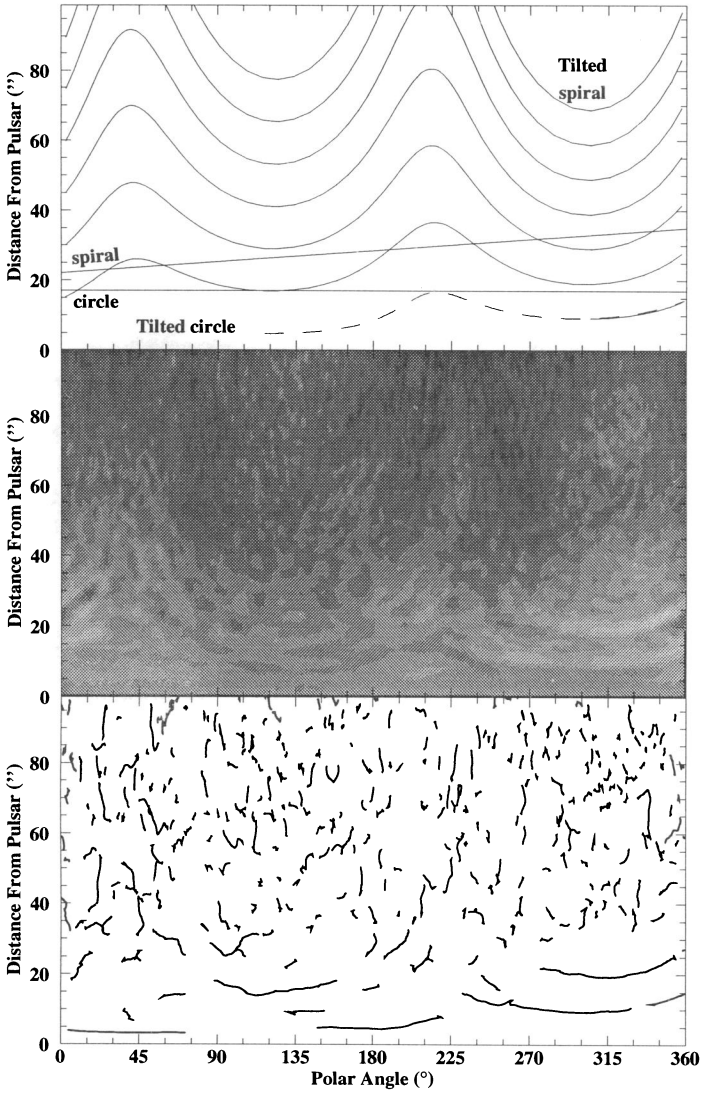

FIG. 2.—(r, θ) representation of the spectral index variations; the angle corresponds to the distance from the pulsar (in arcseconds), and position angle, respectively, of a point in the image. (*Top*) Different curves projected onto the (r, θ) plane. (*Middle*) Projection of the radio α image. The pulsar is at the origin of the polar coordinates. (*Bottom*) Positions of the "ridge lines" of the α image in the (r, θ) plane.

tures, which are ellipse-shaped in projection, have a characteristic "signature" in the (r, θ) plot which is shown by the dashed line in Figure 2. It is clear that the data, at least in part, are in close agreement with the latter geometrical form—see Figure 2*b*. However, we have explored other possibilities: a nonplanar spiral, tilted respect to the line of sight also gives an acceptable fit to the observed features—see Figures 2*b* and 2*c*. We also tried to fit a toroidal geometry to the α features, but we could not find a torus which provided a convincing fit to both the main observed α features. Quantitative comparison of the goodness of fit among these different intrinsic geometrical shapes is complicated. We found the most reliable discriminant to be pattern recognition in the (r, θ) plane.

In our various attempts to fit a simple three-dimensional geometry to the observed α features, one aspect is quite model-independent: the inclination with respect to the plane of the sky is always required to be $\sim 60°$. This suggests that the long axis of the outer nebula is inclined out of the plane of the sky by this amount. The position angle, $\sim 135°$, of the system's axis, is likewise the same for all of the above models. This agrees well with the inclination and position angle of the torus which is seen in X-rays (Aschenbach & Brinkmann 1975) and the position of the pulsar's spin axis as derived from observations of the pulse profile and polarization (Smith et al. 1988).

In Figure 3 we show a comparison with α features which are also visible in new optical images kindly provided by Dr. William Blair. The α features are represented by white lines against the optical continuum image at 477 nm; the image extends $\pm 45''$ from the position of the pulsar and shows that in the majority of the cases, the radio α features lie in *between* the regions of localized maximum optical emission. The geometry of both optical and radio features seems to be similar, both in *curvature* and approximate location, but the optical emitting regions appear to *alternate* with the radio α features in the radial direction.

We have also analyzed the α distribution beyond the limits shown in Figure 2, including the regions coinciding with the "dust bays," located to the east and west of the pulsar, by Fesen et al. (1991). The "dusty bay" regions show a complete *absence* of radio α features.

4. THE COSMIC-RAY ACCELERATION MACHINE

The physical processes in this key, "laboratory" object have been the subject of considerable theoretical analysis (e.g., Piddington 1957; Kardashev 1970; Kahn 1971; Rees & Gunn 1974; Kundt & Krotschek 1980; Kennel & Coroniti 1984a, b; Reynolds & Chevalier 1984; Coroniti 1990; Bietenholz & Kronberg 1991, 1992). A very brief summary of the Crab Nebula's energetics is the following:

The Crab Nebula contains a magnetic field strength 10^{-3}–10^{-4} G and a total energy in relativistic electrons of $\sim 10^{49}$ ergs. These estimates follow from the assumption that the radio, optical, and X-ray continuum is synchrotron radiation (B is not far from the equipartition value). Most of the nonthermal radiated energy flux ($\sim 1.6 \times 10^{38}$ ergs^{-1}) is in the optical to soft X-ray range, where the relevant synchrotron lifetimes are less than the age of the nebula (~ 920 yr). Most of the Crab Nebula's volume (apart from the filaments) is empty of thermal material $n \leq 0.2$ cm^{-3} (Bietenholz & Kronberg 1991).

Since the pulsar is situated in a cavity, all the energy must accumulate within this volume, which expands at a rate $\dot{R}_{\rm neb} \ll c$. A characteristic radius R_S can be designated, at which the ram pressure due to the pulsar's wind $L/(4\pi c R_S^2)$ balances the total magnetic and particle pressure P. Its relation to $\dot{R}_{\rm neb}$ is (Rees & Gunn 1974)

$$\frac{R_S}{R_{\rm neb}} = \left(\frac{\text{light travel time out to } R_S}{\text{age of nebula}}\right)^{1/3} \sim \left(\frac{\dot{R}_{\rm neb}}{c}\right)^{1/2} .$$

The associated shock is located at $\sim 10^{17}$ cm from the pulsar, and it is associated with the wisp region, where the wind energy is randomized. Within this zone, the magnetic field "wound-up" by the pulsar accumulates, and the magnetic energy builds up more rapidly than the particles' energy content.

An interesting and well-known feature of the Crab Nebula is that the region immediately surrounding the pulsar is *underluminous* at radio (Wilson 1972), optical (Schmidt, Angel, &

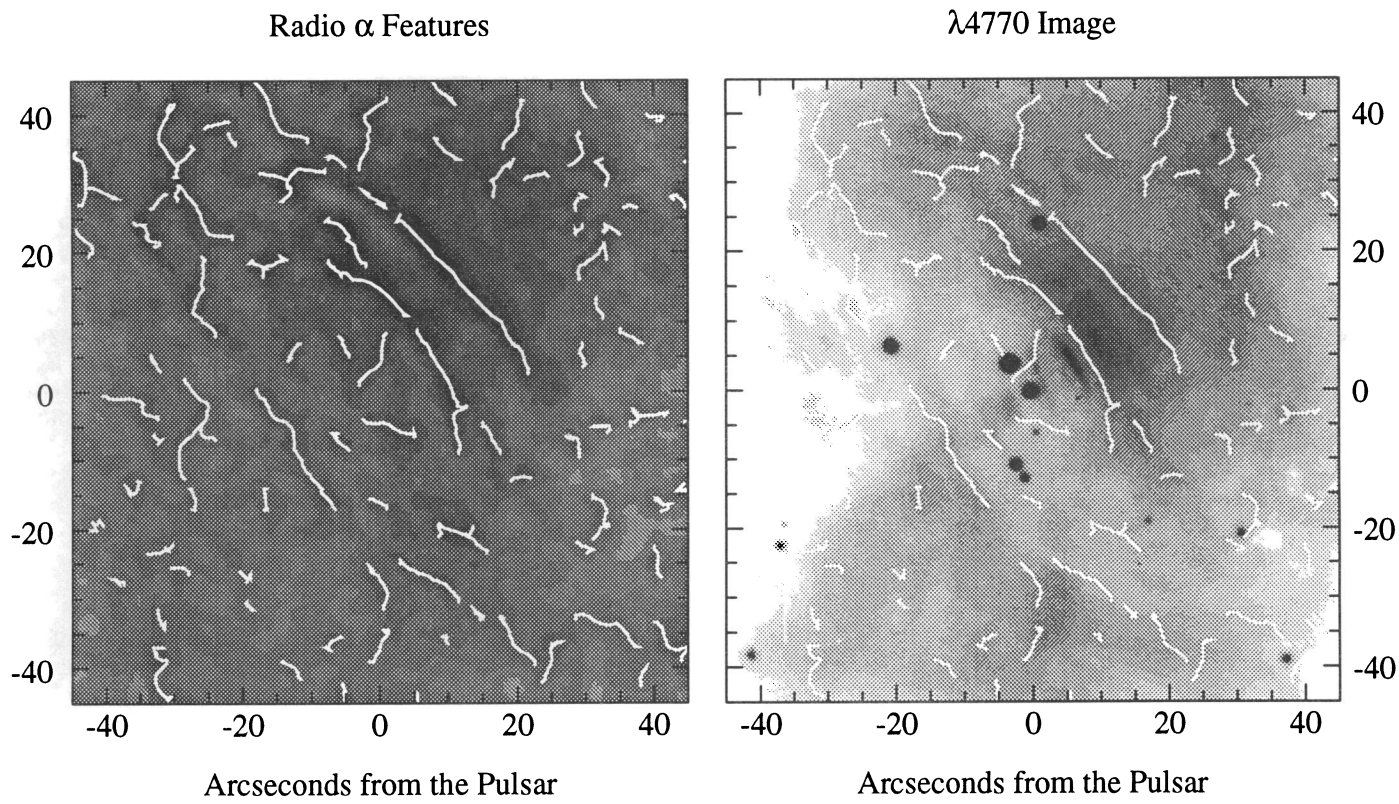

FIG. 3.—*Left:* Radio α map of the inner 45″ from the pulsar with the loci of the maxima overlaid. Right: optical continuum at 4770 Å covering the same area of the sky. α "ridge lines" are represented by the white lines. Optical images courtesy of William Blair.

Beaver 1979), and X-ray (Aschenbach & Brinkmann 1975) wavelengths. The optical surface brightness is only ~10% of that outside an ~20″ × 20″ region, centered on the pulsar. The X-ray emission just *outside* this underluminous region appears to have a toroidal symmetry centered on the pulsar (Aschenbach & Brinkmann 1975; Aschenbach et al. 1992). The original optical wisps—small regions of variable optical brightness—appear to be near the boundary of this underluminous zone.

Given that the pulsar is a source of relativistic particles, the existence of an underluminous region around the pulsar indicates that the streaming particles have almost zero pitch angle. The fact that there is no observational manifestation of the enormous energy flux which must flow through this volume, means that the traditional particle isotropisation mechanism of scattering by Alfvén waves (e.g., as applied to the propagation of cosmic rays through the interstellar medium; Lerche 1967; Kulsrud & Pearce 1969) does not occur here. This emission hole is an indication for the existence of a relativistic wind, as was proposed by Kennel & Coroniti (1984a, b). A positronic wind flows from the pulsar, and the particles and the magnetic field stream with the same velocity. Under these circumstances, no Alfvén waves are excited and no pitch-angle scattering can occur.

4.1. *Propagation and Acceleration of Relativistic Particles in the Crab Nebula*

Most of the nonthermal features in the Crab-nebula (excluding the pulsar itself) can be explained on the basis of a steady spherically symmetric magnetohydrodynamical wind model (Kennel & Coroniti 1984a, b). A highly relativistic positronic wind is terminated by a strong MHD shock wave that decelerates the flow and accelerates particles. This model accounts for the spectral and spatial distribution of the optical to γ-radiation, but does not explain the radio portion of the Crab nebula. However, we will show in the next section that the presence of this termination shock is accompanied by strong excitation of MHD waves, which accelerate electrons and positrons and can explain the observed spectral features and spatial distribution of the radio emission.

Concerning the "wisps" we would like to make some remarks how these features may be directly related with the pulsar itself: wisps are the most prominent features in the optical band. They are variable on time scales of months and have reported to exhibit violent apparent motions of order $0.3c$. If the wisps have enhanced synchrotron emission, then a higher field strength and/or a higher number density of particles is required. Alternatively, we could be seeing beaming effects, since the flow is transrelativistic, and this could possibly be coupled with a nonuniform pitch angle distribution (cf. Arons et al. 1993).

In any case, the optical wisps are features which may be strongly linked to the pulsar. We propose to associate the variability of the optical wisps (roughly months) with the variability of the Poynting flux of the pulsar. If star quakes, or crust quakes, sources of the so-called "glitches" (Ruderman 1969), which may be instabilities in the superfluid neutron star, are able to propagate as Poynting flux disturbances into the nebula, they would need ~4 months to enter the shock region. This is shorter than the observed variability time scale of the

radio wisp features (Bietenholz & Kronberg 1992), but not by as much as an order of magnitude. We propose that the approaching Poynting flux amplifies the magnetic field, which is then convected away from the shock region with the sound velocity in the relativistic plasma, $c/3^{1/2}$. This velocity is indeed very close to the value indicated by the observations. For larger distances from the shock, the velocity should decline to values of less than $0.1c$. The reason for this decrease is that the plasma becomes more and more thermal and the appropriate sound velocity approaches the Alfvén velocity $v_A \sim 0.07c(B/10^{-3}G)(n/10^{-2}\ \mathrm{cm}^{-3})^{-1/2}$, instead of $c/3^{1/2}$.

4.2. *The Radio α-Ridges and Evidence for Acceleration by Alfvén Waves*

Now we attempt to interpret the "radio α-ridges" discovered by Bietenholz & Kronberg (1992). These ridges (Figs. 1 and 2) exhibit flatter radio spectral indices, with $\alpha \sim -0.17$ to ~ -0.12. Allowing for line-of-sight dilution effects, this α perturbation in the radio image suggests that $\alpha \sim +0.0$ *to* $+0.1$ *within the volume of the "α-features."* The projected motion of the ridges has been found to be less than $0.04c$, and close to the Alfvén velocity. In addition, the *absence* of these features has been verified elsewhere within the Crab Nebula by Bietenholz & Kronberg (1992). We will argue that the radio α-ridges are locations of stochastic particle acceleration in which magnetohydrodynamical turbulence, excited by the shock wave, accelerates the electrons and positrons.

A shock isotropizes the directed particle flow originating on the pulsar poles. The isotropization process is provided by Alfvén waves which are generated in the shock layer. The particles are scattered, and the flow velocity is reduced to the local Alfvén velocity (Schlickeiser 1989). It is well known that magnetohydrodynamic (MHD) waves, like Alfvén waves, are likely to accelerate particles to relativistic energies for two reasons: MHD waves can be generated by macroscopic instabilities (shocks, fluid-like instabilities), and they can be resonant with the particles (Achterberg 1981; Eilek & Henriksen 1984; Schlickeiser 1989; Eilek & Hughes 1991). MHD waves affect relativistic particles through their fluctuating electric fields. This interaction is strongest when the waves and the particles are in resonance—which occurs when the wave and particle speeds are well matched, so that energy and momentum transfer are most effective. The fundamental resonance is $\omega - k_{\|} v_{\|} - \Omega_{cr} = 0$, where $k_{\|}$ and $v_{\|}$ are the components of wavenumber and velocity parallel to the magnetic field, and $\Omega_{cr} = eB/(\gamma m_{cr} c)$ denotes the gyrofrequency of a relativistic particle with mass m_{cr} and Lorentz factor γ. Energy and momentum transfer occur because a particle gyrates in phase with the rotating ΔB of a circularly polarized Alfvén wave, so that a coherent Lorentz force persists for many gyrations.

The particle energy gain can be understood as arising from the force of interaction between the particle's magnetic moment and the gradient of the wave electric field, as the particle "rides" the wave. An interesting detail of this acceleration mechanism is that it is effective only if the particle distribution is kept isotropic, by pitch-angle scattering. This is because the rate of energy gain for a particle depends on the component of momentum perpendicular to the magnetic field, but the energy gain all goes to the component which is parallel to the magnetic field (Achterberg 1981). Thus for resonant acceleration to be effective, the particle distribution function should be already isotropized. This is the case if the particles enter a shock wave. A key point is that the final energy will depend on the probability that a particle is in resonance with a wave. In other words, if a particle can easily escape from a region with high wave intensity, it will gain much less energy than a particle which is confined to the wave region.

To summarize, the MHD turbulence not only determines the momentum diffusion coefficient, but it also governs the spatial diffusion coefficient κ. We do not pursue the details here and refer instead to Dröge & Schlickeiser (1986). The essence of their calculations is the following: for particles which are accelerated only by MHD turbulence, the final energy distribution is proportional to E^{-1}, assuming that the spatial diffusion coefficient is independent of particle energy, and that the particles' acceleration time is shorter than their escape time from the wave region. In the terminology of Dröge and Schlickeiser (1986), eq. (16), the applicable parameters are $a = 0$ (no shock acceleration), $\eta = 0$ (momentum independent spatial diffusion), and $\lambda = 0$ (large ratio of escape time to acceleration time). The resulting radiation spectrum is consistent with a synchrotron spectrum having $\alpha \approx 0$, as is observed in the radio ridges (Fig. 1).

Our next consideration is an examination of the conditions under which stochastic acceleration leads to the preferred particle spectrum. First, we discuss the energy dependence of the spatial diffusion coefficient κ. In the last section we argued that κ in the shock is independent of energy, since the particles suffer their first scattering at the shock itself. For radii $R > R_s$ we need to take into account the fact that MHD waves are present. This requires an examination of the microscopic physics of κ, which is the product of the particle velocity times its mean free path l against scattering. It was shown by Schlickeiser (1989) that l is given by

$$l \simeq r_g \left(\frac{L_{\max}}{r_g}\right)^{q-1} \left(\frac{B_0^2}{\delta B^2}\right)^2 .$$

Here $r_g = c/\Omega_{cr}$ denotes the gyroradius of a relativistic particle, q is the spectral index of the MHD turbulence ($q = 5/3$ presents a Kolmogoroff spectrum) and $L_{\max}$ is the maximum dimension of the acceleration region, which we assume to be R_s. It was shown by Achatz, Lesch, & Schlickeiser (1990) that in electron-positron plasmas the excited MHD turbulence spectrum is proportional to k^{-2}, i.e., $q = 2$. We then obtain again $l = R_s$ and κ would be independent of energy. Furthermore, it is known that driven turbulence (which seems reasonable to expect close to a shock wave at which an electron-positron flow arrives), exhibits a k^{-2} spectrum initially (Orszag & Kruskal 1968; Chambers et al. 1988) and results in an initially energy-independent spatial diffusion coefficient. At larger distances from the shock, the turbulence develops into a Kolmogoroff spectrum ($q = 5/3$), and κ starts to depend on the particles' energy via $r_g^{1/3} \propto \gamma^{1/3}$. At this point, the energy distribution changes into a spectrum steeper than E^{-1}, i.e., α negative.

The second relevant phenomenon is acceleration by MHD turbulence alone: in this process, the particles and the turbulence are advected from the shock layer, and the influence on the particle acceleration will decrease.

Third is the important consideration of the ratio of escape time to acceleration time: in our scenario the ridges have an axial magnetic field, which is parallel to the filament axis, i.e., the fllow is at least quasi-perpendicular. The particles can only escape with difficulty since their drift perpendicular to the magnetic field is much smaller than the motion along the field lines.

Therefore the confinement of the particles is very effective, and their escape time is much longer than the acceleration time.

When we incorporate the foregoing three factors into the Crab, we are led to conclude the following: the electrons in the α-ridges are accelerated by MHD waves, which are the cause of the isotropization of the plasma flow in the shock layer. Close to the shock the MHD turbulence has a spectrum which produces an E^{-1} particle spectrum and a radio synchrotron spectral index $\alpha \simeq 0$, as observed. Far away from the turbulence source the resulting particle and synchrotron spectrum will be steeper, also in accord with the observations.

5. MACROSCOPIC COHERENT FEATURES IN THE CRAB NEBULAE

The projected magnetic field within the nebular volume which is outside the filaments was found to have a coherence length of $\sim 10''$ (Bietenholz & Kronberg 1990). We suggest that the fact that this length is close to the inner shock radius, R_s, may be more than coincidental. Laboratory studies of turbulent flows have revealed the existence of *persistence structures*. These structures are advected into the flow and have a size which is comparable to that of the turbulence cell size of the source region, thus "programing" the turbulence far downstream. Such features appear in time-variable turbulent flows, where the pause in the flow occurs over a time scale comparable with the sound crossing time across the source (Hussein 1983, 1986).

In the Crab nebula, the source of turbulence is certainly the shock located at $R_S \sim 3 \times 10^{17}$ cm. If there were considerable turbulence in the plasma wind before entering the shock, the particles would radiate much more. If the shock at R_S experiences changes on time scales larger than the sound crossing time (~ 1 yr), then coherent structures with a scale of $\sim 10''$ should appear. Since the magnetic field at the shock is parallel to the shock plane, the turbulent flow can be expected to generate *persistent structures*, confined by the magnetic field, as is observed in the magnetic field structure of the Crab (Bietenholz & Kronberg 1990).

6. SUMMARY

We have shown that the newly discovered, and time variable radio spectral index perturbations near the center of the Crab Nebula are consistent with a three-dimensional axisymmetric system of circular rings, or possibly a spiral, whose axis is inclined by $\sim 30°$–$40°$ to the plane of the sky. This is consistent with other lines of evidence which indicate that the pulsar spin axis is inclined by a similar amount to the plane of the sky. Beaming may well be able to cause the near side of such structures to be brighter than the far side by factors of ~ 10 and might thus provide an explanation of the one-sidedness of the structures seen in the radio and the optical.

Although the *detailed* explanation of these new features is not clear, it is very likely that they are important sites of relativistic article acceleration. We have shown that a combination of a relativistic wind model and particle acceleration by shock-induced MHD-turbulence reproduces the *spectra* of features seen in the optical, X-ray, and radio, respectively.

The light travel time from the pulsar to the wind shock comprises more than 10^8 pulsar revolutions, which would imply a rather high degree of circular symmetry of the pulsar wind and presumably the associated shock structures at this point. Hoshino et al. (1992) find that a magnetosonic shock in a pulsar wind consisting of electrons, positrons and ions can reproduce the multiple structure of the optical wisps (they are the result of compressional magnetic overshoots) and can also produce the required spectral index in the optical and X-ray range.

What is not yet clear is how the observed double, possibly multiple-ring geometry of the radio ridges arises. The fact that the center of symmetry of the radio wisps seems to be offset from the pulsar indicates that these features are displaced from the pulsar's equatorial plane, and the one-sidedness suggests that the flow velocity at the radio ridges may still be high enough for beaming to suppress the far side of the (presumably) circular features. Better observations of the central region, for example, high-resolution radio observations at several short wavelengths, will be required in order to more unambiguously determine the geometry of the shock region. Because of the time variability of this region, simultaneous radio and optical observations will also be desirable in future.

We acknowledge financial support from the Natural Engineering Research Council of Canada. One of us (H. L.) acknowledges receipt of the Otton Hahn Prize, during whose tenure this paper was written.

REFERENCES

Achatz, U., Lesch, H., & Schlickeiser, R. 1990, A&A, 233, 391
Achterberg, A. 1981, AA, 97, 259
Arons, J., Gallant, Y. A., Hoshino, M., Langdon, A. B., & Max, C. E. 1993, in IAU Colloq. 128, The Magnetospheric Structure and Emission Mechanisms of Radio Pulsars, ed. T. H. Hankins, J. A. Gil, & J. M. Rankin, in press
Aschenbach, B., & Brinkmann, W. 1975, A&A, 41, 147
Aschenbach, B., et al. 1993, in preparation
Bietenholz, M. F., & Kronberg, P. P. 1990, ApJ, 357, L13
———. 1991, ApJ, 368, 231
———. 1992, ApJ, 393, 206
Bietenholz, M. F., Kronberg, P. P., Hogg, D. E., & Wilson, A. S. 1991, ApJ, 373, L59
Chambers, D. H., Adrian, R. J., Moin, P., Stewart, D. S., & Sung, H. J. 1988, Phys. Fluids, 31, 2573
Coroniti, F. V. 1990, ApJ, 349, 538
Dröge, W., & Schlickeiser, R. 1986, ApJ, 305, 909
Eilek, J. A., & Henriksen, R. N. 1984, ApJ, 277, 820
Eilek, J. A., & Hughes, P. A. 1991, in Beams and Jets in Astrophysics, ed. P. A. Hughes, Cambridge Astrophysics Ser. 19 (Cambridge Univ. Press), 528
Fesen, R. A., et al. 1991, preprint
Hoshino, M., Arons, J., Galland, Y., & Langdon, A. 1992, ApJ, 390, 454
Hussein, A. K. M. F. 1983, Phys. Fluid, 26, 2813
Hussein, A. K. M. F. 1986, J. Fluid Mech., 173, 303
Kahn, F. D. 1971, IAU Symposium 46, Changing Trends in Variable Star Search, ed. F. M. Bateson, J. Smak, & I. H. Urch, 281
Kardashev, N. S. 1970, Astr. Zhurn Akad. Nauk. SSSR, 47, 465
Kennel, C. F., & Coroniti, F. V. 1984a, ApJ, 283, 694
———. 1984b, ApJ, 283, 710
Kulsrud, R. M., & Pearce, W. 1969, ApJ, 156, 445
Kundt, W., & Krotscheck, E. 1980, A&A, 83, 1
Lerche, I. 1967, ApJ, 147, 689
Orszag, S. A., & Kruskal, M. D. 1968, Phys. Fluids, 11, 43
Piddington, J. 1957, Australian J. Phys., 10, 530
Rees, M. J., & Gunn, J. E. 1974, MNRAS, 167, 1
Reynolds, S. P., & Chevalier, R. A. 1984, ApJ, 278, 630
Ruderman, M. A. 1969, Nature, 223, 597
Scargle, J. D. 1968, in Supernovae and their Remnants, ed. P. J. Bracanzio & A. G. W. Cameron (New York: Gordon & Breach), 197
———. 1969, ApJ, 156, 401
Schlickeiser, R. 1989, ApJ, 336, 243
Schmidt, G. D., Angel, J. R., & Beaver, E. A. 1979, ApJ, 227, 106
Smith, F. G., Jones, D. H. P., Dick, J. S. P., & Pike, C. D. 1988, MNRAS, 233, 305
Wilson, A. S. 1972, MNRAS, 157, 229